



ELSEVIER

Contents lists available at ScienceDirect

Thin-Walled Structures

journal homepage: www.elsevier.com/locate/tws

Review

Experimental and numerical buckling analysis of a thin TRC dome

E. Verwimp^{a,b,*}, T. Tysmans^a, M. Mollaert^b, S. Berg^a^a Vrije Universiteit Brussel, Faculty of Engineering, Department of Mechanics of Materials and Constructions (MeMC), Brussels, Belgium^b Vrije Universiteit Brussel, Faculty of Engineering, Department of Architectural Engineering (ARCH), Brussels, Belgium

ARTICLE INFO

Article history:

Received 23 December 2014

Received in revised form

26 February 2015

Accepted 13 March 2015

Keywords:

Buckling

Experimental investigation

Finite elements

Modified Riks method

Shell structures

Textile reinforced concrete (TRC)

ABSTRACT

Shells in textile reinforced concrete (TRC) can be made very thin thanks to their non-corroding reinforcement. Consequently, buckling becomes an important parameter. Because of the lack of data in literature, this paper presents the experimental and numerical analysis on the buckling behaviour of a TRC dome (2 m span, 0.2 m height, 3.7 mm thick), which is subjected to a uniform pressure load until it buckles. This experiment is simulated using the Riks method in Abaqus and implementing geometrical imperfections. The simulations correspond well to the experimental data and validate the model, which enables the prediction of buckling, necessary when designing thin TRC shells.

© 2015 Elsevier Ltd. All rights reserved.

Contents

1. Introduction	2
2. Experimental investigation	2
2.1. Textile reinforced concrete: material choices	2
2.2. Geometry and production of a TRC shell	2
2.3. Experimental instrumentation and test set-up	3
3. Experimental results	3
3.1. Deflection–pressure behaviour	4
3.2. Strain–pressure behaviour	4
3.3. Failure behaviour	6
4. Numerical model	6
4.1. Model build-up	6
4.2. Introduction of geometrical imperfections	6
4.3. Non-linear analysis	7
5. Comparison experimental results to finite element simulation	7
5.1. Pressure–displacement behaviour	7
5.2. Strain evolution	7
6. Conclusions	8
References	9

* Corresponding author. Tel.: +32 2 629 29 27; fax: +32 2 629 29 28.

E-mail address: everwimp@vub.ac.be (E. Verwimp).

1. Introduction

The persistent investigation of cementitious composites in recent years led to the development of strain hardening materials with high compressive and tensile strength, ductility and energy absorption. By combining continuous fabrics with a fined grain matrix a material, known as textile reinforced concrete (TRC), is obtained. Because the textile is flexible enough to copy the shape of any mould, strongly curved and complex shell shapes can be obtained, as demonstrated in [1,2]. Because of the relatively good mechanical properties of TRC and the non-corroding reinforcement, TRC shells can be executed (very) thin. This was recently proven at RWTH Aachen University, where a pavilion composed of four hypar TRC shells [3,4] was successfully constructed. Each shell, produced as a precast part, is supported at its centre by a steel reinforced concrete column. The 6 cm thick shells, reinforced with 12 layers of a non-corroding textile reinforcement of carbon fibres, have a base area of 7×7 m and are arranged in a 2 by 2 grid, resulting in a pavilion of 14×14 m and showing the potential of TRC structures.

The higher the slenderness of TRC shell structures, the more they are prone to buckling. While buckling of steel reinforced concrete shells is relatively well examined and general design rules were developed throughout the years [5–7] this is not the case for textile reinforced concrete shells. The slenderness TRC shells can achieve is far superior than that of steel reinforced concrete shells. It should therefore be studied whether the same methodology may be used for those very thin shells. In the literature no experimental data exist on buckling of TRC shells. For this reason, this paper presents the experimental and numerical investigation of the buckling behaviour of a TRC dome. The spherical dome (2 m span; 0.2 m high; 3.7 mm thick) is subjected to a uniform pressure until it fails under buckling (Fig. 1).

The first part of the paper describes the experimental methodology, i.e. the shell geometry tested, the used materials, the manufacturing of the shell and the test setup. The experimental results, containing not only the failure behaviour but also the strain evolution at various locations as a function of the applied pressure, are discussed in detail. The second part of the paper compares this experiment to a numerical analysis using the modified Riks method, performed in the finite element software Abaqus. The influence of geometrical imperfections on the

buckling behaviour is studied and linked to the experimental observations.

2. Experimental investigation

2.1. Textile reinforced concrete: material choices

In the study presented in this paper, the matrix Inorganic Phosphate Cement (IPC) [8], developed at Vrije Universiteit Brussel, is used in combination with E-glass fibre mats. Just like other cements, unreinforced IPC is brittle; the compressive strength equals approximately 80 MPa, while the tensile strength is at least 10 times smaller and lies between 6 and 8 MPa [9]. The stiffness of IPC equals 18 GPa. IPC is chosen as matrix because it has very small grain size – thus good impregnation of a dense textile is possible – and because it becomes pH neutral after hardening – thus can be used with glass fibres. The textile used in this study is a chopped E-glass fibre mat with a density of 300 g/m^2 (Fig. 2(a)). This random oriented fibre mat is chosen over a bidirectional textile, because it is the aim to build not only domes but also more complex shell geometries, in which the forces work in all different directions rather than in two principal directions. Although the chosen materials are not those of traditional textile reinforced concrete, the mechanical material behaviour of glass fibre textile reinforced IPC (GFTR-IPC) on a macro-scale is analogue to that of TRC. The used chopped fibre mats provide a continuous reinforcement just like textiles, and as the used matrix allows us to impregnate a high fibre volume fraction, the resulting composite shows a significant strain hardening in tension. For this reason, we choose to refer to GFTR-IPC as a kind of TRC.

The mechanical behaviour of GFTR-IPC differs significantly in tension and compression due to the brittle matrix. In compression GFTR-IPC is assumed to be linear until failure [9], but in tension it shows already a non-linear behaviour at low tensile stresses due to the low tensile failure strain of the matrix relative to that of the fibres (Fig. 3(a)). However, by adding high fibre volume fractions the composite can obtain a significant post-cracking stiffness and tensile strength (Fig. 3(b), [10]). The properties of the glass fibre textile reinforced IPC can be found in Table 1.

2.2. Geometry and production of a TRC shell

To perform the experimental investigation a simple and well known shell geometry is chosen, namely a spherical dome. Because of restrictions in our lab, a dome of 2 m span, 0.2 m height and with a radius of curvature of 2.6 m is studied. The thickness of the dome must be well chosen to ensure that the dome will fail due to buckling instability during testing rather than

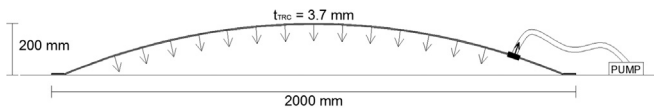


Fig. 1. The spherical dome (2 m span; 0.2 m high; 3.7 mm thick) is subjected to a uniform pressure by means of a vacuum pump.

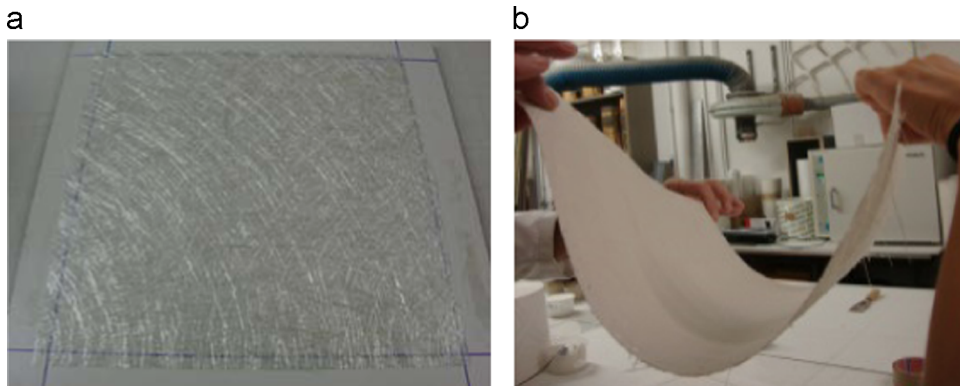


Fig. 2. By impregnating the chopped E-glass fibre mat (a) with Inorganic Phosphate Cement, a flexible composite is obtained (b) as long as the cement is wet.

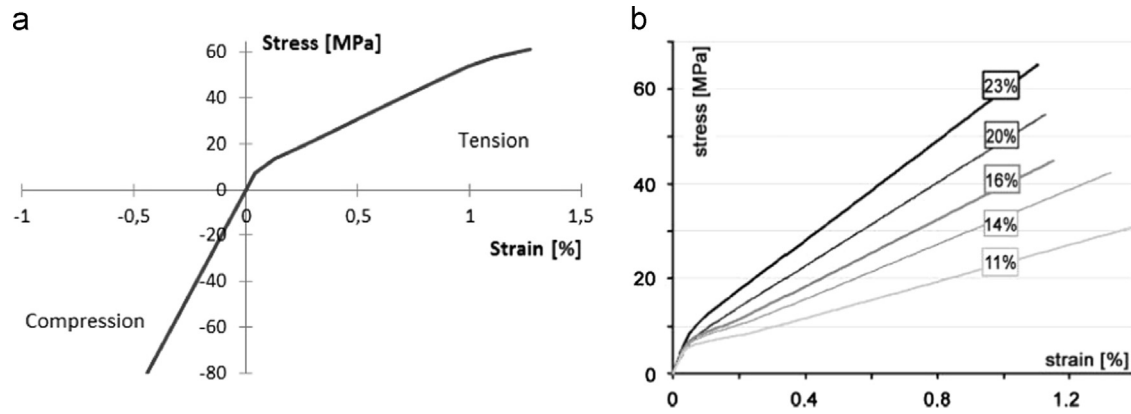


Fig. 3. GFTR-IPC is linear in compression and non-linear in tension (a) [11], increasing the fibre volume fraction of the glass fibre mats increases its post-cracking stiffness and tensile strength (b) [10].

Table 1
Properties of glass fibre reinforced Inorganic Phosphate Cement.

Quantity	
Density	$\rho = 1750 \text{ kg/m}^3$
Compressive characteristic strength	$\sigma_{ck} = 80 \text{ MPa}$
Tensile characteristic strength	$\sigma_{tk} = 40 \text{ MPa}$
Initial E-modulus	$E_{c1} = 18 \text{ GPa}$
Fibre volume fraction	$V_f = 18\%$
Poisson ratio	$\nu = 0.3$

failure by excessive stresses. In other words, the main goal of the experiment is to emphasize on the failure of the structure by the instability phenomenon. Based on the experimental set-up of [12], which focusses on the buckling behaviour of plain concrete domes with a radius of curvature to thickness ratio $\lambda_{sl} = 385$, it is decided to manufacture a dome which is even more slender. Therefore a 3.5 mm thick shell is targeted, resulting in a $\lambda_{sl} = 722$. Moreover, Young's modulus of the GFTR-IPC material is lower (18 GPa) than the one of (normal) concrete (30 GPa), i.e. the GFTR-IPC dome would be even more prone to buckling than the concrete shell in [12], even when taking the same slenderness ratio. Taken into account these two factors, the dome is designed to fail in buckling.

To make sure the wanted geometry is precisely fabricated, a polystyrene foam mould is milled according to the dimensions of the spherical dome (accuracy of around 1 mm on the radius of curvature and 5 mm on the span). In this foam mould the TRC dome is built up. The fibre textiles, composed of randomly oriented chopped E-glass fibre mats, are cut in half circles to fit perfectly one-half of the polystyrene mould. After the mats are placed into the mould (Fig. 4(a)), they are impregnated with the IPC matrix by hand lay up (Fig. 4(b)). Seven layers of mats are put on top of each other and impregnated, targeting a thickness of 3.5 mm. Because one layer of the shell contains two identical mats next to each other around a symmetry line, a small overlap (approximately 1 mm) will be present between the two mats. To limit the influence of this overlap to the buckling behaviour, the two mats of the next layer are positioned in such a way that the overlap between these two mats makes an angle of 45° with the overlap of the previous two mats. When all the layers are set, the shell is covered with a thin plastic veil and hardens at ambient temperatures for 24 h. After 24 h, the shell is cured with heating carpets (60°C) to make sure that the GFTR-IPC is totally hardened. Finally, after hardening, the GFTR-IPC shell is removed from the mould and inverted (Fig. 4(c)). The maximum measured section thickness – 4.7 mm – is located at the three overlaps, where locally 9 layers of fibre mats are placed instead of 7. However, this local thickening of the section does not increase the buckling load of the

TRC dome. The determining thickness is the minimal measured thickness of the section, namely 3.7 mm.

2.3. Experimental instrumentation and test set-up

The next paragraphs describe the test set-up of the GFTR-IPC dome (Fig. 5). Firstly, the loading application is explained and secondly, the measurement equipment is presented.

The GFTR-IPC dome is subjected to a uniform distributed load by creating an underpressure between the shell and the concrete floor in the lab. In order to be able to remove the air between the dome and the concrete floor, a hole is drilled in the dome and a connection is designed to attach the hose of the vacuum pump to the shell in such a way that no air can leak. The hole is drilled 20 cm from the edge of the dome, in order to avoid local failure of the structure around the fixation of the pump hose. To measure the radial pressure applied on the shell, a pressure meter is placed diametrically to the vacuum pump. Between the concrete floor and the GFTR-IPC dome a rubber is placed to prevent leakage of air through these zones.

The base of the GFTR-IPC dome is free to move in all directions at the edge except along the vertical axis, thus the structure is not maintained laterally. Since tension will occur in the edge under this loading pattern, the edge is reinforced with carbon fibre strips which are glued onto the shell border with an epoxy resin, to avoid premature failure of the edge instead of the buckling instability. The carbon strips do not form one continuous tension ring around the shell and do not restrict the horizontal directions.

In order to follow the evolution of the strains in specific locations on the shell, two sets of five strain gauges (locations 1–5 in Fig. 5) are placed on the central line at the top and bottom surfaces of the structure. Bidirectional strain gauges are used, where the index 'M' stands for the strains in the meridian direction and 'H' in the hoop direction.

In combination with the strain gauges, a digital image correlation (DIC) system is used in order to obtain the displacement fields and strains in the experimental shell. For this experiment two sets of two cameras are used to register the displacement and strains in the dome on two locations of $400 \times 500 \text{ mm}$, i.e. one zone monitoring the centre of the structure and another near the edge (dotted rectangles in Fig. 5).

3. Experimental results

The next paragraphs describe the results which were monitored with the strain gauges and the digital image correlation.



Fig. 4. The GFTR-IPC dome is produced in layers. (a) First, the fibre mats are placed in the foam mould. (b) Second, the mats are impregnated with the matrix IPC. (c) After hardening, the dome is inverted and a thin GFTR-IPC shell is obtained.

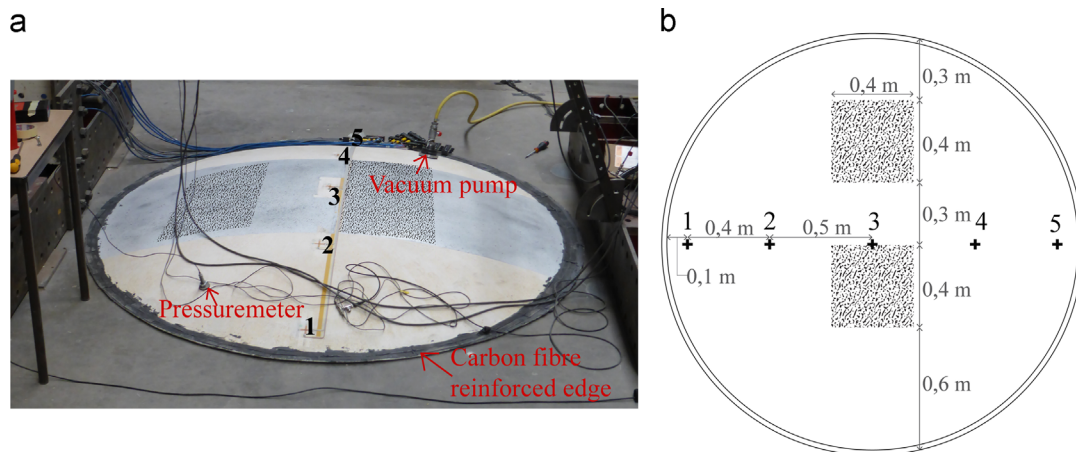


Fig. 5. The GFTR-IPC dome is subjected to a pressure and reinforced at the edge with carbon fibre strips. The experiment is monitored by strain gauges and digital image correlation.

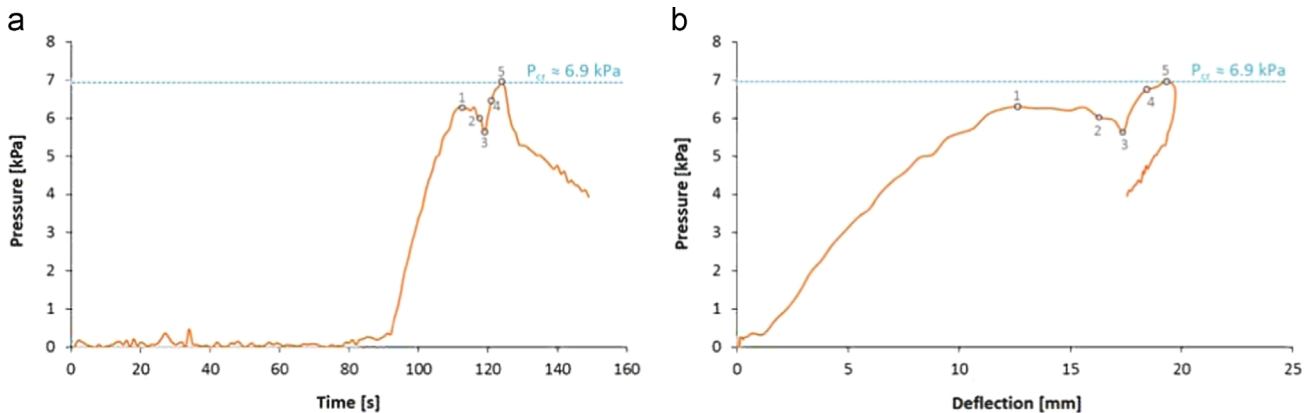


Fig. 6. The pressure–deflection (at the centre) increases monotonically until the pressure load decreases because of cracking and air leakage. Finally, the load increases again until the shell buckles at the critical load of 6.9 kPa.

3.1. Deflection–pressure behaviour

First of all, the pressure evolution as a function of time (Fig. 6 (a)) is studied in order to highlight some important events which occurred during testing; this evolution is put next to the graph which displays the deflection of the centre as a function of the pressure (Fig. 6(b)). Five markers are chosen in the graph at different time steps, which will come back in the next graphs. As seen in Fig. 6(a), the pressure increases monotonically until it reaches approximately 6.2 kPa (point 1), where a small pressure decrease occurs ($\Delta p = 0.6$ kPa, from point 1 to 3), presumably the result of cracking and air leakage at the edge. The pressure–

deflection relation increases monotonically until this point of cracking and air leakage (point 1 in Fig. 6(b)). From here on, the shell deflects further without pressure increase. From point 3 on, the pressure increases again until the critical load of 6.9 kPa is reached and the structure buckles near the edge (Fig. 7).

3.2. Strain–pressure behaviour

In the next paragraphs the strain behaviour is discussed as a function of the pressure increase.

Fig. 8(a) shows the strains at the shell edges – at locations 1 and 5. As shown in Fig. 8(a), the top surface near the edge shows

compressive strains in the meridian direction (M1top and M5top) up to 4250 $\mu\text{m}/\text{m}$. The bottom surface (M5bottom) has tensile strains which reach up to 3850 $\mu\text{m}/\text{m}$. This indicates the bending behaviour near the edge of the shell. The general trend of the strains on both the top and bottom surface is similar but opposite. The strains on both locations 1 and 5 have only a small discrepancy and follow the same trend, proving the axisymmetry of the shell. The strains in the hoop direction on the top surface (H1top and H5top) are in compression and show similar behaviour at both

monitored edges with strains up to 350 $\mu\text{m}/\text{m}$. The strain on the bottom surface (H5bottom) also indicates a bending trend near the edge as this strain differs from the strain on the top surface. Furthermore, the strains in the hoop direction evolve linearly until shortly before failing (350 $\mu\text{m}/\text{m}$). Towards the end of the test, at a pressure of 6.2 kPa on location 1 (H1top), the hoop strain decreases about 80 $\mu\text{m}/\text{m}$ (from point 1 to 3), which means the shell is progressively converting compressive stresses into tensile stresses. This phenomenon announces the buckling of the GFTR-IPC dome near the edge.



Fig. 7. The shell buckles locally near the edge.

Fig. 9 focuses on the strains at about quarter span of the shell. These strains at locations 2 and 4 both in meridian and hoop direction are much smaller (maximum 100 $\mu\text{m}/\text{m}$) than the strains near the edge. Averagely, the meridian strains (Fig. 9(a); M2top and M4top) evolve linearly with increasing pressure before cracking and air leakage occurs (before point 1). The hoop strains (Fig. 9 (b)) are both in compression and also show a linear development. Here, the strains show to be the same over the thickness (H4top and H4bottom) before cracking and air leakage, demonstrating that the entire section is in compression. Afterwards, the strain falls back during the pressure drop (points 1–3) and then increases with the same slope as the initial one, until buckling. The strains on the same axisymmetric position (H2top and H4top) are slightly

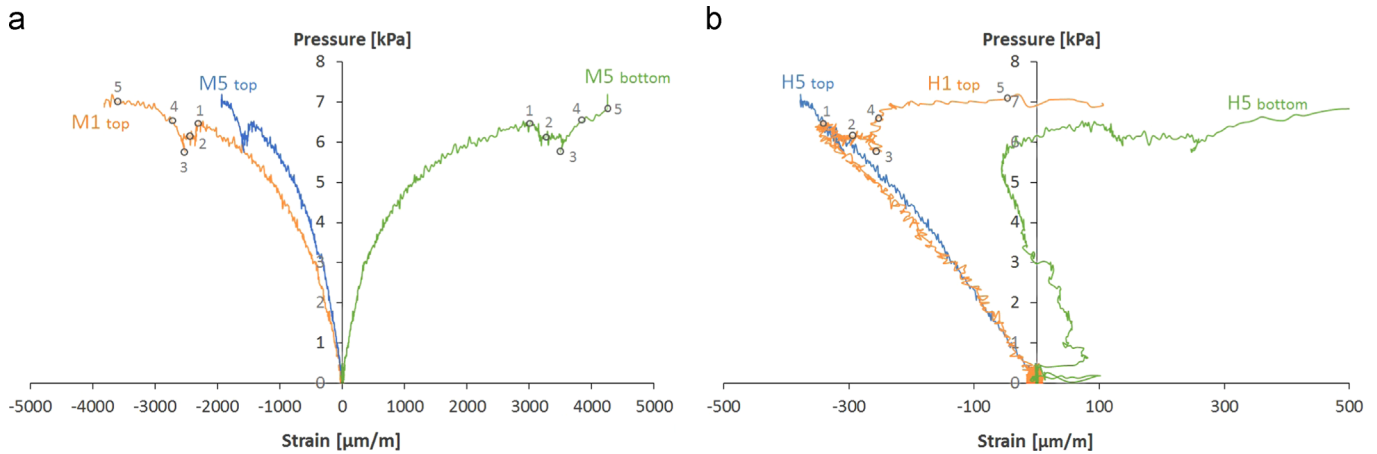


Fig. 8. Strains at the shell edges – location 1 and 5. Both the strains in the meridian direction (a) and hoop direction (b) indicate the bending behaviour in the Section. The strains on positions 1 and 5 correspond very well, showing the axisymmetric behaviour of the dome.

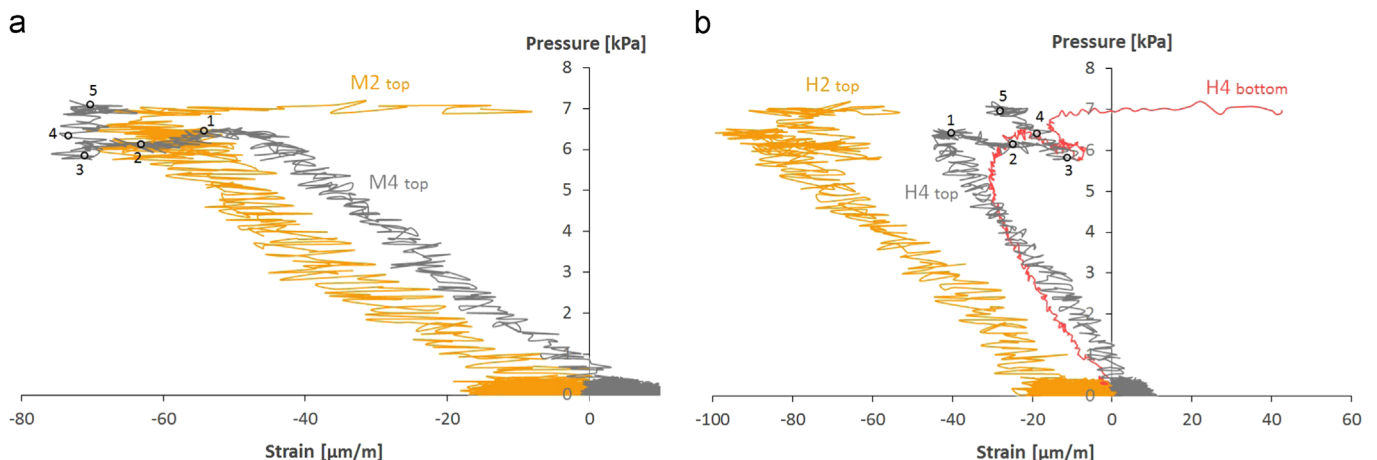


Fig. 9. Strains at about quarter span of the shell – locations 2 and 4. The strains demonstrate that the entire section is in compression, however they also show the non-perfect axisymmetry of the shell.

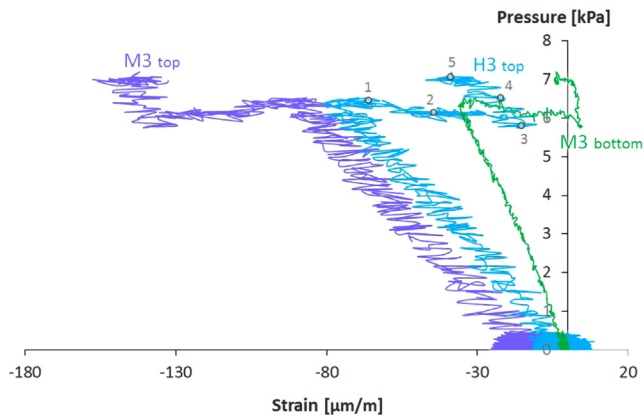


Fig. 10. The strains at the shell centre – location 3 – indicate a combination of compression and bending.

shifted, however they show the same trend and have the same order of magnitude.

As Fig. 10 shows, the strains on the top surface at the centre of the dome are similar in the meridian and hoop direction since the shell is axisymmetric. In fact, the hoop direction at the centre corresponds in this case to a meridian line which is perpendicular to the initial meridian. The top surface of the shell centre shows compressive strains which increase linearly up to 80–100 $\mu\text{m}/\text{m}$. However, the strains at the bottom surface are still in compression but significantly lower, showing a combination of compression and bending at the shell's centre. The structure, which is laterally not supported, behaves in the meridian direction like an arch where the thrust forces are barely taken up, inducing bending at the edges and at the top of the shell.

3.3. Failure behaviour

In general the behaviour of the dome is as expected before cracks initiate at the edges and air leakage occurs (point 1). When the cracks appear the axisymmetry is lost and it is unpredictable what happens. The maximum measured compressive strain reached at buckling is approximately 3850 $\mu\text{m}/\text{m}$ at location 1 in meridian direction (Fig. 8 (a)), this means a stress of 69.3 MPa, which is 86.6% of the compressive failure strength (80 MPa).

Fig. 11 shows the vertical deformations of the shell over the meridian perpendicular to the meridian line where the strain gauges were placed (locations 1–5). The full line represents the area captured by the DIC cameras, the dotted line was obtained by curve fitting. The deformations are shown for different load steps. Up till the load of 5 kPa the dome deforms approximately symmetrically and almost linearly with increasing load. At the failure load of 6.9 kPa the deformation is strongly asymmetric and equals 25 mm near one edge ($=L/80$). This large deformation proves the dome failed indeed because of buckling and not because of excessive stresses. The maximal tensile strain reached is approximately 4250 $\mu\text{m}/\text{m}$ (also at location 1 in meridian direction), which equals a stress of 27.3 MPa and is 68.3% of the tensile failure strength (40 MPa).

The compressive strains at all other locations are a lot smaller and do not even exceed 150 $\mu\text{m}/\text{m}$, which means a stress of 3 MPa. The tensile strains on the other locations are almost non-existing and are far below the elastic limit of the GFTR-IPC material of 400 $\mu\text{m}/\text{m}$. After the elastic limit in tension is reached, the cement matrix starts to crack and the behaviour of the material is no longer linear. This phenomenon is visible in the curve of Fig. 8(a) in meridian direction, where around 400 $\mu\text{m}/\text{m}$ the slope of the curve changes from the linear curve, which corresponds to a pressure of 3.2 kPa.

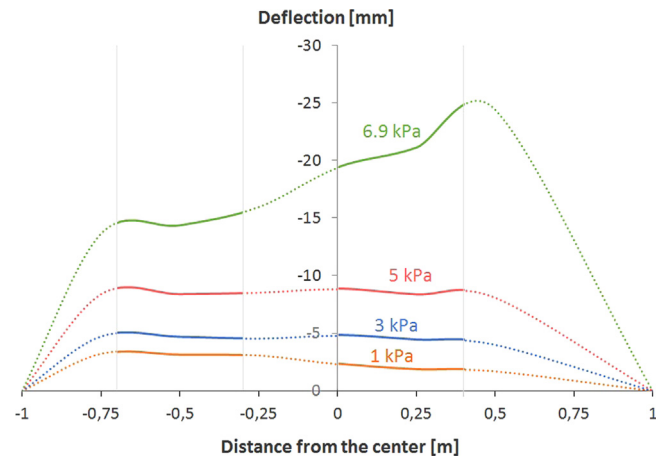


Fig. 11. The deformation over a line in the DIC zone is asymmetrical and the large deformations indicate buckling.

4. Numerical model

The experiment is simulated using the finite element (FE) software Abaqus and the experimental results are compared with the numerical ones. The analysis is based on Riks' arc-length technique with implementation of geometrical imperfections in the dome.

4.1. Model build-up

The dome is modelled as a shell model with a continuous shell section. Two types of linear elements are used, namely the triangular S3 and the quadrangular S4R elements, standing for 3-node shell elements and 4-node shell elements with reduced integration respectively. They are both three-dimensional general-purpose elements which can be used for both thin and thick shells in all kinds of boundary conditions and loading conditions [13]. Mostly the S4R elements are used, but if locally the geometry of the shell does not allow them, S3 elements are used instead. Mesh convergence was checked for this shell geometry; a sweep mesh with 7106 elements is chosen, which seems most suitable in terms of accuracy and calculation time.

The GFTR-IPC material behaviour is assumed linear elastic in this simulation. Including the non-linearity of the material in tension would decrease the stiffness of the shell model, as ongoing research has shown. However, considering the high slenderness of the shell, geometrical non-linearities will be predominant in a buckling simulation. As the results in Section 5.1 will show, a linear elastic material assumption allows for a fast yet adequately close prediction of the buckling load, which justifies the linear material model assumed in this paper.

The shell's edge is only restricted in the vertical direction and the carbon reinforcement, which was glued on the edge during the experiment, is not taken into account in the FE simulation. The spherical dome is loaded with a uniform pressure and the shell's self-weight is not taken into account, because the weight of the very thin shell (3.7 mm \Rightarrow 65 Pa) is negligible compared to the pressure load which is applied (up to 9 kPa).

4.2. Introduction of geometrical imperfections

Real shells are built and executed with imperfections; the same holds for the lab-manufactured shell. These imperfections can reduce enormously the buckling resistance of shells [14] and therefore geometrical imperfections are introduced in the FE model. Very often, the shape of the first buckling mode of the eigenvalue buckling

analysis is taken as the initial imperfection [6,14]. However, shells with closely spaced buckling loads are highly sensitive to geometrical imperfections, and there is no physical reason why another buckling mode would not induce buckling faster than the first mode. For this reason, other buckling modes than the first and combinations of different buckling modes are also taken as the initial imperfection in this study. Medwadowski [5] recommends to use the value of the shell thickness as an order of magnitude for geometrical imperfections for concrete structures as a rather conservative limit and thus an imperfection size equal to 100% of the GFTR-IPC dome thickness (3.7 mm) is considered.

4.3. Non-linear analysis

In case of buckling simulation of thin structures, it is important to consider the non-linear behaviour coming from geometrical non-linearities. Along this paper, a non-linear analysis is performed using the modified Riks method – a load–deflection method – in Abaqus [13]. The Riks method uses the load magnitude as an additional unknown, and solves the problem simultaneously for loads and displacements. The loading during a Riks step is always proportional. The current load magnitude, P_{total} , is defined by

$$P_{total} = P_0 + \lambda(P_{ref} - P_0) \quad (1)$$

where P_0 is the dead load (in our case the neglected self-weight), P_{ref} is the reference load vector, and λ is the load proportionality factor. The load proportionality factor is found as part of the solution, and printed at each increment. The solution is a single equilibrium path in a space defined by the nodal variables and the loading parameter, and the actual load value may increase or decrease as the solution progresses.

5. Comparison experimental results to finite element simulation

5.1. Pressure–displacement behaviour

Firstly, the pressure–displacement of the centre curve of the experiment is compared to the numerical results assuming a geometrical imperfection size of 3.7 mm (100% thickness) and with different imperfection shapes (Fig. 12(a)). Extracted from a linear eigenvalue buckling analysis, following geometrical imperfections and combinations are considered: Mode 1, mode 2, a combination of modes 2 & 3 and a combination of modes 4 & 5. As seen in Fig. 12(a), the numerical pressure–displacement of the centre curves depends significantly on the considered imperfection shape, i.e. the buckling

mode which is assumed. The buckling pattern obtained in the numerical analysis of the dome with the geometrical imperfection based on mode 2 (Fig. 12(b)) corresponds best to the failure pattern which was observed during the experiment (Fig. 7). The dome with this geometrical imperfection based on buckling mode 2 also fits the pressure–deflection graph the best and the value of the maximum pressure load (numerically 7.5 kPa; experimentally 6.9 kPa) is well predicted. Therefore, in the following paragraph the experimental results are compared to the numerical results with mode 2 as geometrical imperfection, in order to validate the model. When designing such a shell however, the lower limit has to be considered to ensure that the calculated load bearing capacity of the structure is sufficient.

5.2. Strain evolution

The discrepancy between the numerically determined and experimentally measured strain at location 1 (shell edge) at the top surface in the meridian direction (Fig. 13 (a)) is relatively small, i.e. a root-mean-square error (RMS) of 214 $\mu\text{m}/\text{m}$ whereas the maximum reached strain goes up to 4000 $\mu\text{m}/\text{m}$. The numerical model thus predicts well the experimental behaviour at location 1 in the meridian direction. The strain evolution numerically determined at location 1 in the hoop direction (Fig. 13(b)) shows a small increase of the compressive strain whereas the experimental curve exhibits larger strain values for the same pressure level. The RMS error equals 325 $\mu\text{m}/\text{m}$, which is a large difference because the experimental strains reach up to only 350 $\mu\text{m}/\text{m}$. However, the general trend of both curves is relatively similar.

The strain prediction at around a quarter span on the top surface (Fig. 14(a) location 2) in the meridian direction is overestimating the experimental values with a RMS error of 28 $\mu\text{m}/\text{m}$, however until a pressure of approximately 3 kPa the curves do correspond. Starting from this value, cracks are initiated at the edge which can explain this discrepancy. The strains have in both cases the same order of magnitude and remain below 150 $\mu\text{m}/\text{m}$. The strain evolution in the hoop direction on the other hand is almost perfectly predicted by the numerical model with an RMS error of 8 $\mu\text{m}/\text{m}$. The global behaviour is similar both in the strain ascending part and the decreasing part for strains which remain below 100 $\mu\text{m}/\text{m}$.

The strain at the top surface of the shell's centre is very well predicted as the RMS error equals only 9 $\mu\text{m}/\text{m}$. The slope is not exactly the same, but the general behaviour is a lot alike (Fig. 15).

In general, the numerical model seems to be representative for the experiment as all strains, except for the strain in hoop

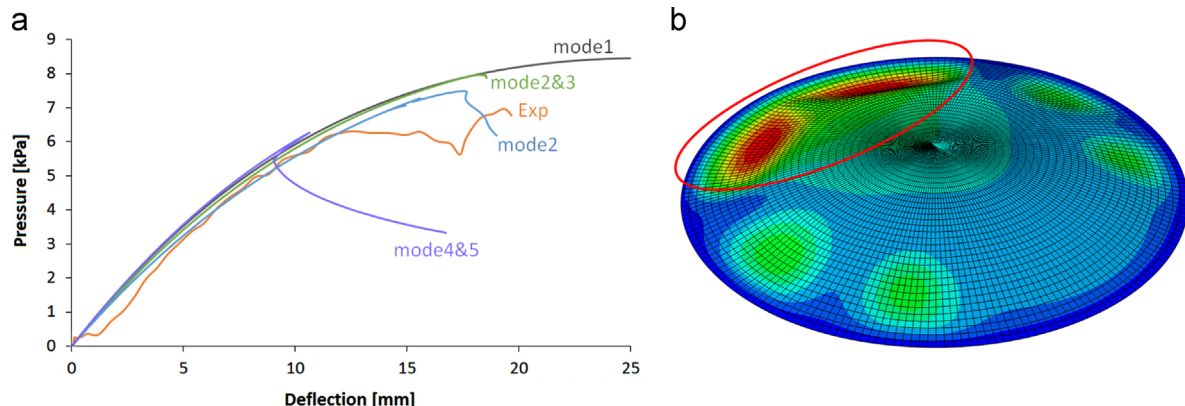


Fig. 12. The pressure–deflection of the centre relation (a) and the buckling pattern (b) of the numerical model correspond best to the experiment when a geometrical imperfection based on the linear buckling mode 2 is used.

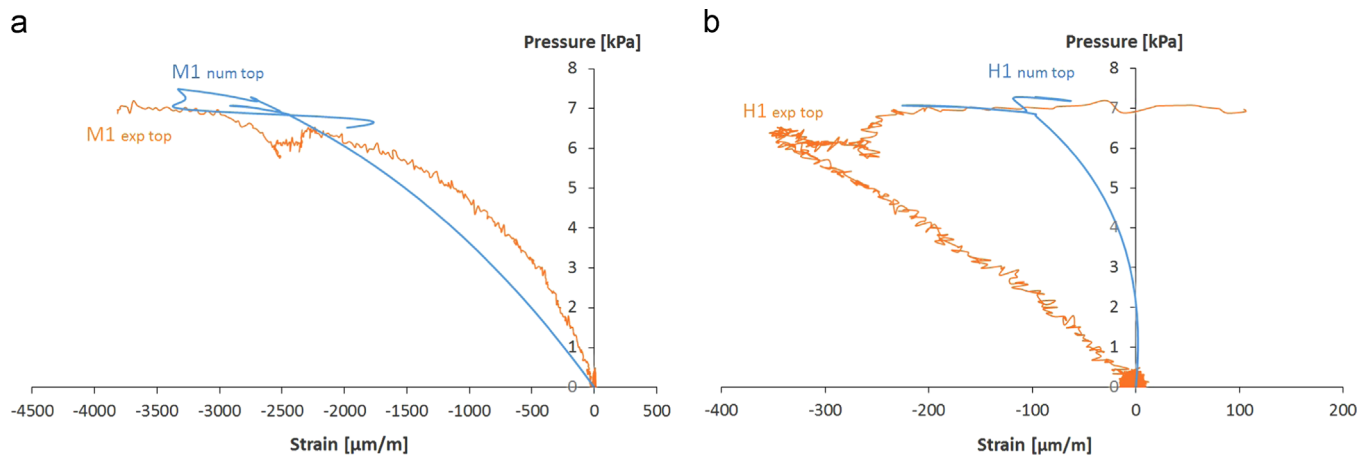


Fig. 13. Strains near the edge – location 1. The strain in the meridian direction (a) is relatively well predicted by the numerical model while the strain in the hoop direction (b) differs a lot in value but follows the same trend.

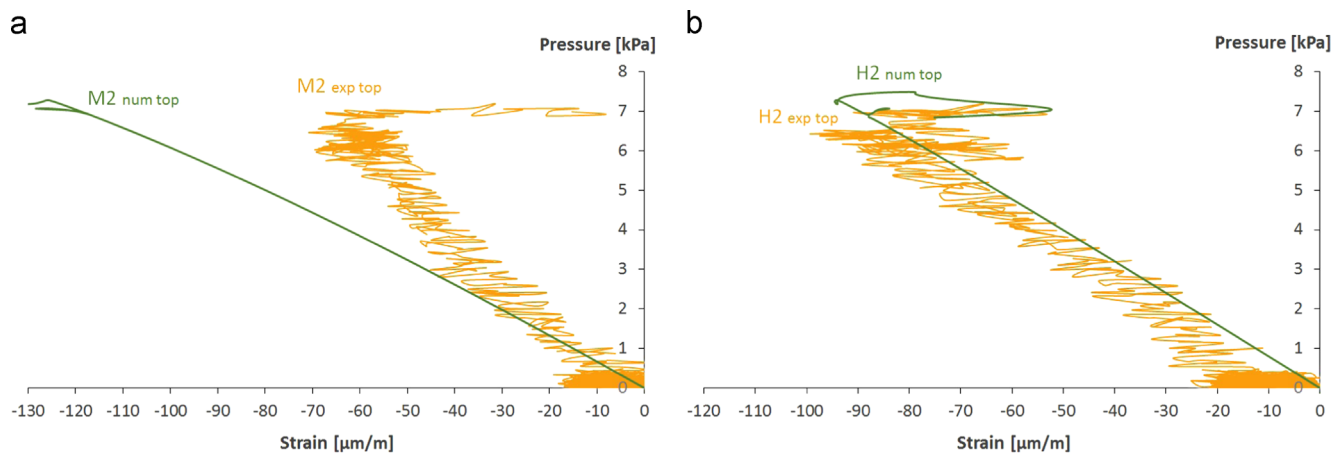


Fig. 14. Strains at around quarter span – location 2. The strain in the meridian direction (a) is a little bit overestimated by the numerical model while the strain in the hoop direction (b) is almost perfectly predicted.

direction on location 1 (edge), have the same order of magnitude and the global trend is similar for all curves. The buckling behaviour is thus relatively well predicted, both for the value of the maximum pressure load and for the load–displacement path and the strains.

6. Conclusions

This paper studied the production and testing to failure of a shallow thin-walled GFTR-IPC dome under uniform (internal) pressure. The dome had a base diameter of 2 m, a thickness of 3.7 mm and a radius of curvature to thickness ratio of $R/t = 722$. To understand the structural behaviour of the GFTR-IPC dome, it was monitored during testing with strain gauges and digital image correlation. The experiment was successfully performed and results indicated that the failure of the GFTR-IPC dome was the result of asymmetrical buckling – which was the aim – at the edge affected by the bending effect and imperfections.

The dome, subjected to uniform pressure, showed structural behaviour as expected. The top surface was completely in compression both in the meridian and hoop direction, with the maximum values near the edge (locations 1 and 5). On the bottom surface, tensile strains were measured near the edge in both directions, but predominantly in the meridian direction. Comparing the strains on the top and bottom surface, bending was present at the centre

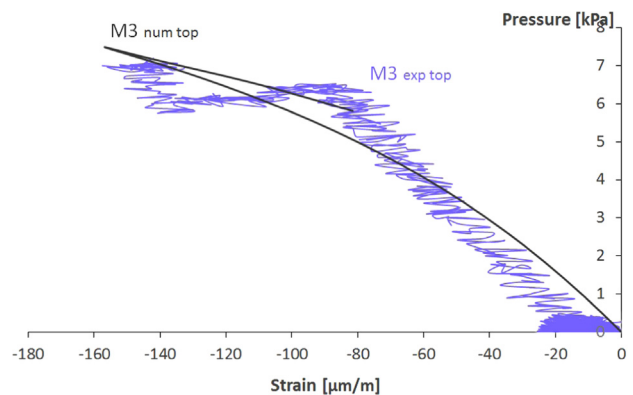


Fig. 15. Strains at the centre – location 3 – are well predicted and show both a similar trend and value.

(location 3) and near the edge. The maximum observed tensile strain in the shell is $+4250 \mu\text{m}/\text{m}$ which corresponds to a stress of 27.3 MPa (68.3% of the tensile failure strength) and the maximum compressive strain equals $-3850 \mu\text{m}/\text{m}$ which correspond to a stress of 69.3 MPa (86.6% of the compressive failure strength). Furthermore, the deformation near the edge at the failure load (6.9 kPa) equals 25 mm ($=L/80$) and showed a strongly asymmetrical profile along the shell, proving the shell failed because of buckling instability.

The experiment was simulated using the Modified Riks method in Abaqus. The buckling behaviour highly depends on geometrical imperfections, and more specifically on the imperfection shape (i.e. the assumed buckling modes), but it is not known in advance how 'imperfect' the shell will be and which imperfection mode is determining. When designing thin TRC domes, the most critical case must be considered. However, to model this experiment, observation allows us to select the buckling mode which corresponds to the actual geometrical imperfections in the manufactured shell. As such, the experiment can be compared to the model with the correct imperfection assumption. The maximum pressure load, the pressure–deflection of the centre curve and all strains, except those in the hoop direction near the edge (location1), are very well estimated by the numerical model both in order of magnitude and trend. For this reason, the model is validated for this experiment and the buckling behaviour of thin TRC domes can be predicted.

These interesting results encourage us to continue the research on the buckling behaviour and design of GFTR-IPC shells. Based on the used numerical model, other geometries than domes and other load patterns should be examined, enabling the design of complex GFTR-IPC shell geometries which will be realised in the future.

References

- [1] Ehlig D, Schladitz F, Frenzel M, Curbach M. Textile concrete: an overview of executed projects. *Beton- und Stahlbetonbau* 2012;107:777–85.
- [2] Tysmans T, Adriaenssens S, Wastiels J, Remy O. Textile reinforced cement composites for the design of very thin saddle shells: a case study, In: Proceedings of the 18th International Conference on Composite Materials, Jeju Island, South Korea; 2011.
- [3] Scholzen A, Chudoba R, Hegger J. Thin-walled shell structure made of textile reinforced concrete Part I: structural design and realization. *Struct Concr—Journal of the Fib* 2014;24.
- [4] Scholzen A, Chudoba R, Hegger J. Thin-walled shell structure made of textile reinforced concrete Part II: experimental characterisation ultimate limit state assessment and numerical simulation. *Struct Concr—Journal of the Fib* 2014;27.
- [5] Medwadowski SJ. Buckling of concrete shells: an overview. *J Int Assoc Shell Spat Struct* 2004;45(144):131–48.
- [6] Dulacska E, Kollar L. Design procedure for the buckling analysis of reinforced concrete shells. *Thin Walled Struct* 1995;23:313–21.
- [7] Andres M, Harte R. Buckling of concrete shells: a simplified numerical approach. *J Int Assoc Shell Spat Struct* 2006;47(3).
- [8] EP 0 861 216 B1. Inorganic resin compositions. Their preparation and use thereof.
- [9] Cuypers H. Analysis and design of sandwich panels with brittle matrix composite faces for building applications [Doctoral thesis]. Brussel, Belgium: Vrije Universiteit Brussel; 2001.
- [10] Remy O. Lightweight stay-in-place formwork: a concept for future building applications [Doctoral thesis]. Brussel, Belgium: Vrije Universiteit Brussel; 2011.
- [11] Wozniak M, Tysmans T, Vantomme J. Finite element modelling of glass fibre reinforced composites with Inorganic Phosphate Cement matrix: comparison of inbuilt Abaqus concrete models. In: Proceedings of the 19th international conference on composite materials, Montréal, Canada; 2013.
- [12] Chang ZT, Bradford MA, Gilbert RI. Short-term behaviour of shallow thin-walled concrete dome under uniform external pressure. *Thin-Walled Struct* 2011;49:112–20.
- [13] Abaqus 6.12-1 documentation. Chapter 6: analysis procedures, solution, and control, Section 6.2.4: unstable collapse and postbuckling analysis. In: Abaqus analysis user's manual.
- [14] Reitingner R, Ramm E. Buckling and imperfection sensitivity in the optimization of shell structures. *Thin-Walled Struct* 1995;23(1–4):159–77.